CONSTITUTIVE MODELING FOR ISOTROPIC MATERIALS

Ulric S. Lindholm and Kwai S. Chan
Southwest Research Institute
San Antonio, Texas

This report covers the fourth and final year of a HOST project with the initial objective "to develop a unified constitutive model for finite element structural analysis of turbine engine hot section components." During the first three years of this project, two existing models of the unified type were further developed for application to isotropic, cast, nickel-base alloys used for air-cooled turbine blades and vanes. The two models are those of Walker (ref. 1) and of Bodner and Partom (ref. 2). Both models were demonstrated to yield good correlation with experimental results for two alloys: PWA alloy B1900+Hf and MAR-M247. The experimental correlations were made with testing under uniaxial and biaxial tensile, creep, relaxation, cyclic, and TMF loading conditions over a range in strain rates and temperatures to 1100°C. Also, both models were entered into the MARC finite element computer code with test cases run for a notched round tensile specimen and an airfoil portion of a typical cooled turbine blade. The airfoil was exercised through three full flight spectra of taxi, take off, climb, cruise, descent, taxi, and shutdown. Computational efficiency with the unified models was as good or better than with a more classical elastic-plastic approach. Significant difference in stress range and accumulated strain after three flight cycles was shown for the unified models when compared with the classical creep-plasticity models. Previous work has been reported in references 3-5.

The final year's work to be reported on herein has been primarily involved with the study of nonisothermal problems and the potential for thermal history effects to occur explicitly in the constitutive equations. The following discussion will present the results from this work.

THERMO-MECHANICAL CONSTITUTIVE TESTS

Experimental Setup

The thermo-mechanical test specimens were of tubular geometry, heated externally by induction heating, and cooled by forced air over both the external and internal surfaces. Mechanical loading in tension or compression was provided by an MTS closed-loop hydraulic machine. Total strain was measured with a ceramic reach-rod extensometer with 25.4 mm gage length. A dynamic temperature monitoring (thermocouple) and control system was developed to compensate in real time for thermal strains based on measured nonlinear thermal expansion coefficients. In the thermo-mechanical test, the thermal strain signal is summed with the prescribed mechanical strain signal for total strain

feedback control. Test results are presented in terms of mechanical strain only. Controlled temperature response curves are shown in figure 1 indicating typical heating and cooling rates. Most experiments were performed in the range from 538°C to 982°C.

Nonisothermal Tensile Tests

Experiments and analysis were performed with B1900+Hf in monotonic tensile loading with a ramp change in temperature ($\dot{T}$ = 4.4°C/sec) at approximately 1% strain. A uniform strain rate of 10^{-4}/sec was maintained throughout the loading. Figures 2 and 3 show the experimental and computed (Bodner-Partom model) results. The experiments indicate negligible thermal history effect in that for either increasing or decreasing temperature change the isothermal hardening curve is achieved rapidly after the temperature change is completed. The B-P model calculation is similar, however a preliminary yield type behavior is observed with an asymptotic approach to the isothermal hardening curve. However, this predicted behavior is not the result of thermal history but of the plastic work history, since cumulative plastic work is used as the measure of the hardening state variables in this model.

Nonisothermal Creep

Creep testing was performed with step changes in both stress and temperature during a given test. An example strain-time curve is shown in Figure 4. After each change, conditions were held until a steady state creep rate was achieved. The steady-state creep rates are plotted in figure 5 for both isothermal and nonisothermal histories along with the B-P model prediction. The isothermal and nonisothermal tests are seen to fall within the same scatter and both agree rather well with the model. In the model, thermal recovery of hardening is insignificant at 760°C but becomes a major factor at 982°C. The nonisothermal testing was designed to include this transition in hardening mechanism.

Thermo-mechanical Strain Cycling

In figure 6, we show a single specimen cycled to saturation initially at 538°C, a temperature increase to 982°C with saturated loops achieved at that temperature, and a return to 538°C, all under constant strain range control. Two observations again evidence absence of thermal history effect. The high-temperature excursion resulted in no change in the hysteresis loop at 538°C, and the cyclic stress range associated with a given cyclic strain was the same under this type of nonisothermal history as under strictly isothermal cycling, as shown in Figure 7. Both types of cycling agree with the B-P model prediction which is based on isothermal data only.

Additional in-phase and out-of-phase TMF cycling experiments were also performed with the cyclic loop shape compared with B-P model predictions. The results were similar to those previously reported in reference 5, indicating that reasonably good predictions of complex nonisothermal histories can be

made for this class of alloy based upon material constants derived from isothermal testing only. For other alloys, where strong strain aging effects are present, more complex thermo-mechanical history dependence may be required in the constitutive model as reported by Robinson and Bartolotta in reference 6.

Dislocation Structures

The dislocation structures observed in the nonisothermal specimens were compared to those observed in isothermal specimens previously reported by Moreno et al in reference 7. The comparison revealed that in both cases the dislocation arrangements in B1900+Hf consisted of cellular networks around the γ' precipitates. Such dislocation cell structures appear to form at low strain levels (a few percent) and appear to be the stable configuration for specimens tested under different loading paths. The theoretical implication is that the saturation stress concept postulated in many unified constitutive models can be considered to be the flow stress associated with the saturated dislocation configuration, i.e., the stress required to move dislocations to and from the walls of the dislocation cellular network. Since the saturated dislocation structure is independent of the thermo-mechanical loading path, the saturation stress and the limiting values of the internal hardening variables should therefore be independent of the thermo-mechanical loading path. The values of the saturation stress should, however, depend on temperature and strain rate through the dependence of the critical resolved shear stress on these quantities.

CONCLUSIONS

The last year's efforts have demonstrated that for the cast nickel-base alloys studied, B1900+Hf and MAR-M247, both isothermal and nonisothermal, complex loading histories can be well predicted using the unified constitutive model approach with all necessary material constants derived solely from isothermal test data. Additional work is needed to determine if this conclusion can be extended to other alloy systems which may exhibit more complex hardening or recovery mechanisms.

We believe the complete four-year program has demonstrated rather conclusively that the unified constitutive model concept is a very powerful tool for predicting material response in hot section components under complex, time-varying, thermo-mechanical loadings. This confidence is gained from extensive correlations between two existing models and a large base of experimental data covering the range in stress, strain rate, and temperature of interest. The unified constitutive models have also been demonstrated to be computationally efficient when incorporated into a large finite element computer code (MARC). While there is still much room for improvement or extension of the existing constitutive models and for efficiency in their computational implementation, it is expected their use will grow rapidly in engineering applications.

REFERENCES

1. Walker, K. P.: NASA CR-165533, 1981.

2. Bodner, S. R.; and Partom, Y: ASME J. of Applied Mechanics, Vol. 42, 1975, p. 385.

3. Lindholm, U. S.; Chan, K. S.; Bodner, S. R.; Weber, R. M.; Walker, K. P.; and Cassenti, B. N.: NASA CR-174718, May 1984.

4. Lindholm, U. S.; Chan, K. S.; Bodner, S. R.; Weber, R. M.; Walker, K. P.; and Cassenti, B. N.: NASA CR-174980, July 1985.

5. Chan, K. S.; Lindholm, U. S.; Bodner, S. R.; Hill, J. T.; Weber, R. M.; and Meyer, T. G.: NASA CR-179522, August 1986.

6. Robinson, D. N.; and Bartolotta, P. A.: NASA CR-174836, 1985.

7. Moreno, V.; Nissley, D. M.; and Lin, L. S.: NASA CR-174844, 1985.

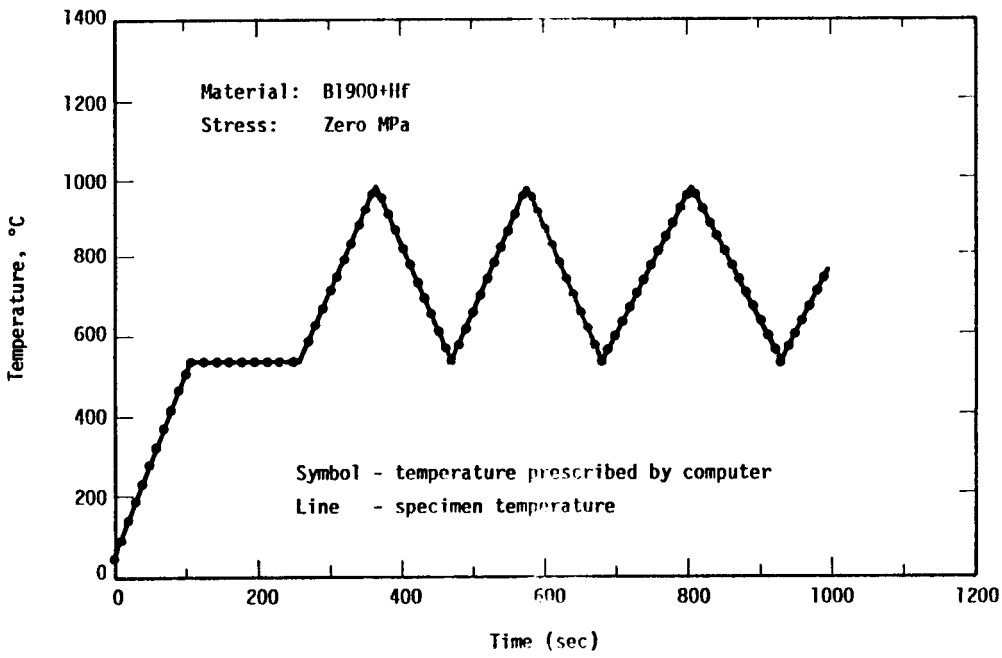

FIGURE 1. COMPARISON OF PRESCRIBED TEMPERATURE WITH MEASURED SPECIMEN TEMPERATURE

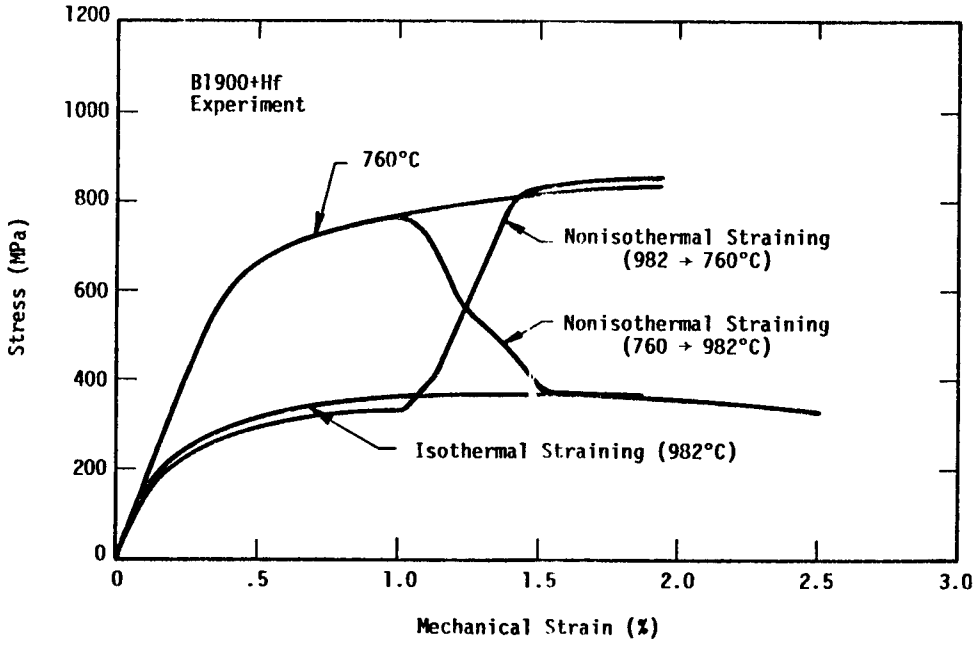

FIGURE 2. EXPERIMENTAL ISOTHERMAL AND NONISOTHERMAL TENSILE STRESS-STRAIN CURVES

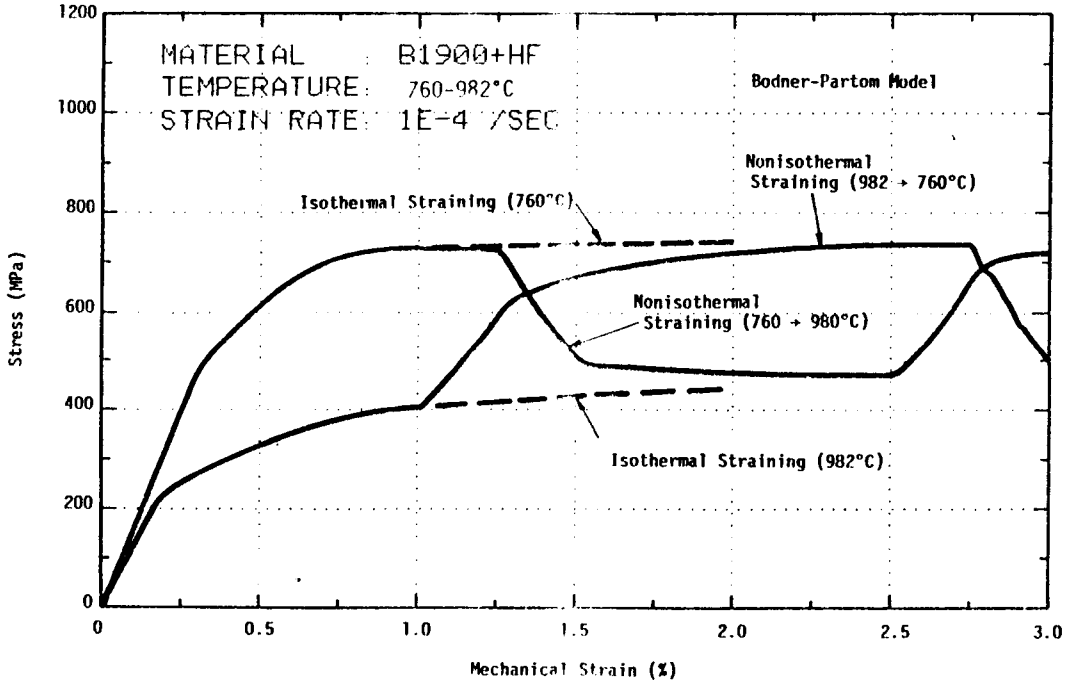

FIGURE 3. BODNER-PARTOM MODEL PREDICTIONS OF NONISOTHERMAL TENSILE CURVES COMPARED TO ISOTHERMAL TENSILE CURVES

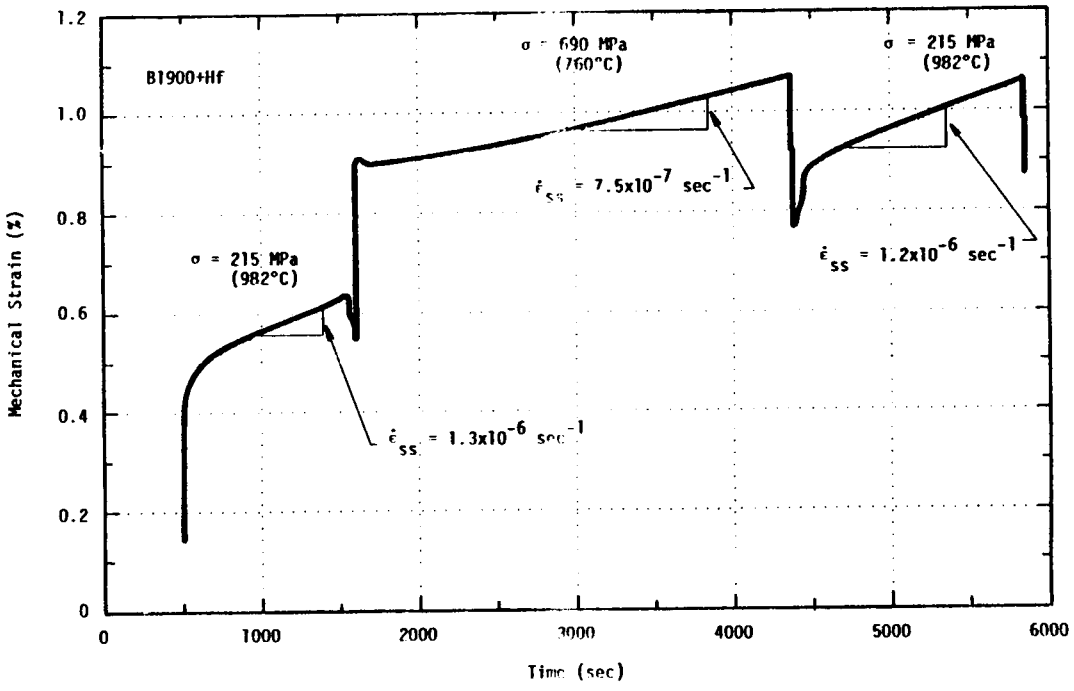

FIGURE 4. CREEP TEST WITH STEP CHANGES IN LOAD AND TEMPERATURE

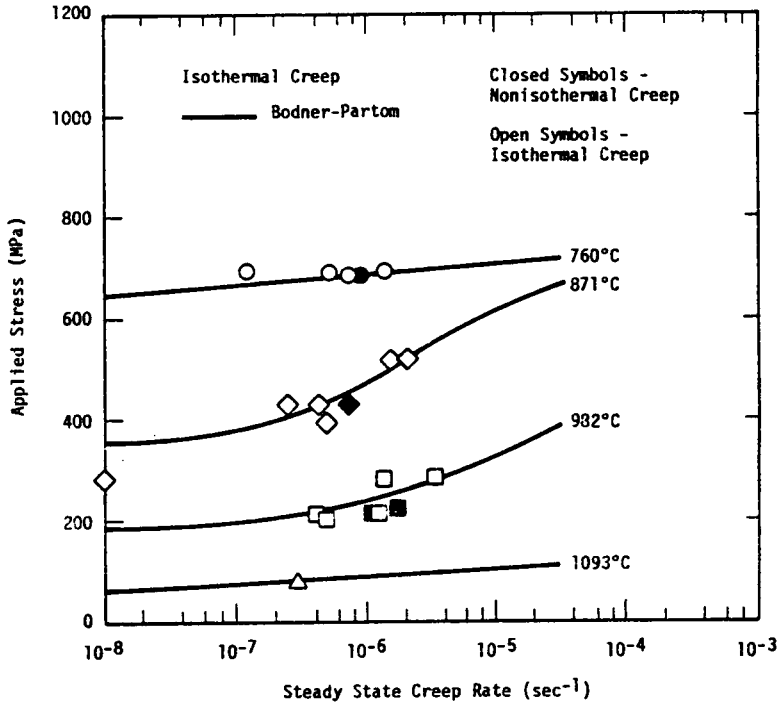

FIGURE 5. COMPARISON OF NONISOTHERMAL CREEP DATA WITH ISOTHERMAL CREEP DATA AND MODEL PREDICTIONS

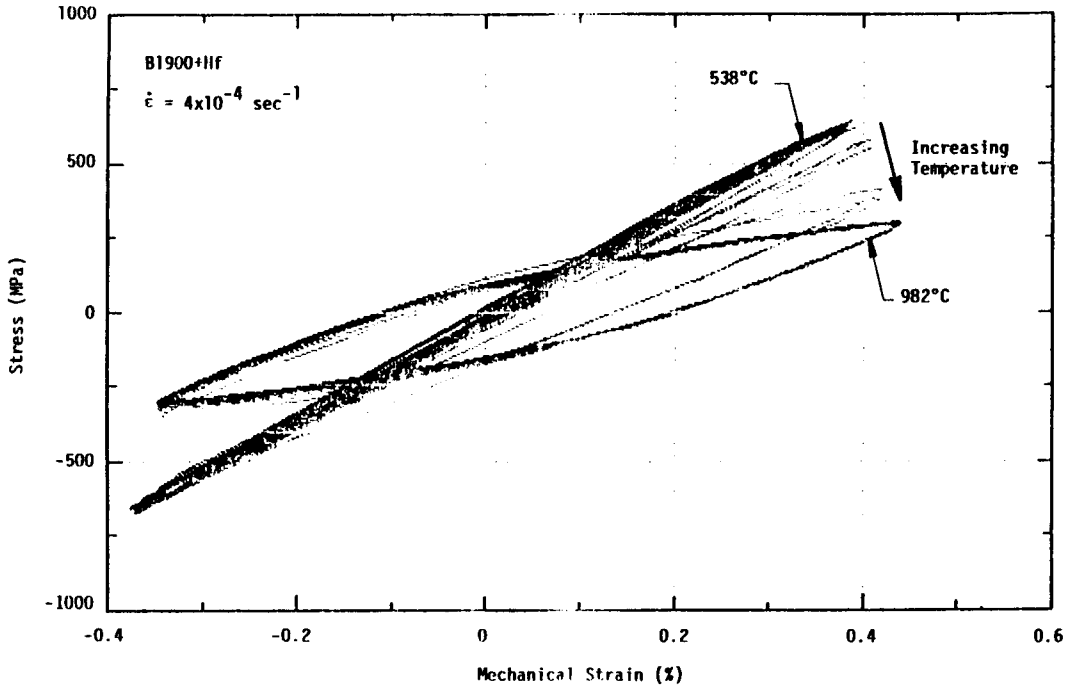

FIGURE 6. CONTROLLED STRAIN CYCLING WITH TEMPERATURE CHANGE FROM 538°C TO 982°C TO 538°C

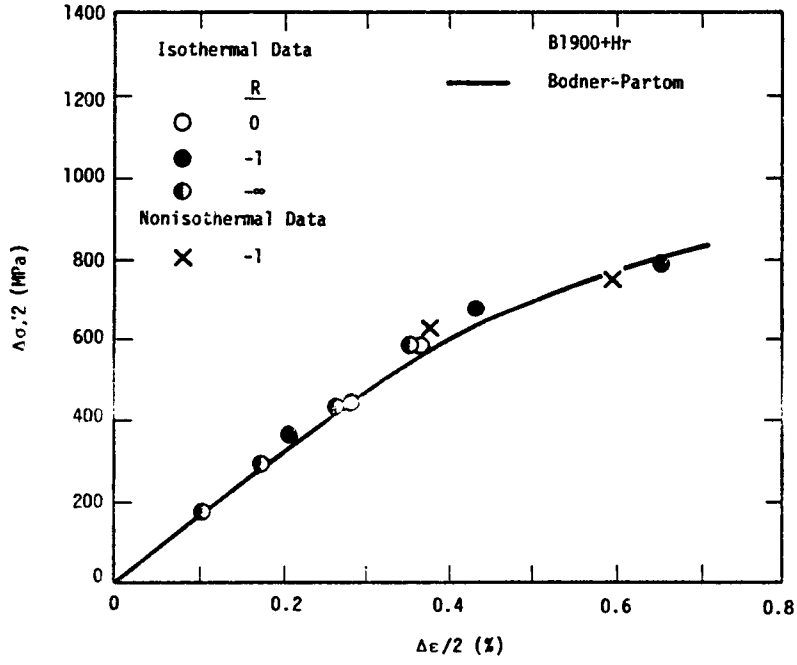

FIGURE 7. COMPARISON OF ISOTHERMAL AND NONISOTHERMAL CYCLIC DATA OF B1900+Hf AT 760°C